NOLTA, IEICE

Paper

Quantization robustness from dense representations of sparse functions in high-capacity kernel associative memory

Akira Tamamori [1]

[1] *Faculty of Information Science, Aichi Institute of Technology*
1247 Yachigusa, Yakusa-cho, Toyota-shi, Aichi 470-0392, Japan

arXiv:2604.20333v3 [cs.NE] 8 May 2026

Received October 27, 20XX; Revised December 29, 20XX; Published July 1, 20XX

Abstract: High-capacity associative memories based on Kernel Logistic Regression (KLR) achieve strong retrieval performance but typically require substantial computational resources. This paper investigates the compressibility of KLR Hopfield networks to clarify the geometric principles underlying their robust representations. We present a geometric interpretation based on spontaneous symmetry breaking and Walsh analysis, and examine it through compression experiments involving quantization and pruning. The experiments reveal a clear asymmetry: the network remains robust under low-precision quantization while exhibiting strong sensitivity to pruning. We interpret this behavior through a "sparse function, dense representation" principle, in which a sparse input mapping is implemented through a dense bimodal parameterization. These findings suggest a practical route toward hardware-efficient kernel associative memories and provide insight into the geometric principles underlying robust representation in neural systems.

Key Words: kernel associative memory, quantization robustness, distributed representation, representational duality, Walsh analysis

1. Introduction

Associative memory models, epitomized by the Hopfield network, have recently attracted renewed interest through the integration of modern machine learning techniques. In particular, our recent work showed that Kernel Logistic Regression (KLR) learning substantially enhances storage capacity and robustness, achieving performance beyond classical limits [1, 2]. These "kernelized" memories operate by embedding patterns into a high-dimensional feature space, forming deep attractor basins. Furthermore, we theoretically identified a geometric self-organization mechanism, termed *Spectral Concentration* [3], that underlies this high-capacity behavior.

In parallel with these developments, model compression has become a major research topic in deep learning. Recent advances in Large Language Models have demonstrated that aggressive quantization, such as 4-bit or even 1.58-bit representations (e.g., BitNet [4]), can preserve performance while substantially reducing computational cost. Whether similar compression principles apply to kernel-based associative memories, however, remains largely unexplored.

Addressing this question is important because the high performance of KLR Hopfield networks comes at a substantial computational cost. Retrieval in kernel networks requires computing weighted sums over all stored patterns using high-precision dual variables, leading to considerable computational and memory overhead. This poses a practical challenge for deployment on resource-constrained edge devices and neuromorphic hardware, where memory bandwidth and

This work is licensed under a Creative Commons Attribution Non Commercial, No Derivatives 4.0 License.

energy efficiency are critical. In contrast, biological neural systems are known to operate efficiently with noisy, low-precision synaptic weights and distributed representations. This raises a central question: Does high-capacity associative memory fundamentally require high-precision continuous parameters, or can the essential information be represented in a more robust and discrete form? More broadly, what geometric structure governs this representation?

In this study, we investigate the compressibility of KLR Hopfield networks from this perspective. We systematically analyze the effects of two forms of compression: *Uniform Quantization* (reducing bit precision) and *Magnitude Pruning* (inducing sparsity). Our experiments reveal a clear dichotomy in the network's compressibility. The network remains highly robust to quantization, maintaining near-perfect recall accuracy even at 2-bit resolution. In contrast, it is highly sensitive to sparsification, with performance degrading rapidly even under moderate pruning.

Our work provides a geometric interpretation of this dichotomy, connecting the empirical compression behavior with the structure of the learned representation. The main contributions of this paper are as follows:

1. We identify a dichotomy in the compressibility of KLR Hopfield networks: robustness to quantization and sensitivity to sparsity.
2. We develop a unified geometric interpretation of this behavior based on two complementary observations: the emergence of a bimodal, digital-like weight distribution and a Walsh analysis that reveals sparse functional structure together with distributed parameterization.
3. We support this interpretation through extensive experiments and discuss its implications for hardware-efficient neuromorphic computing.

The remainder of this paper is organized as follows. Section 2 reviews related work on model compression and distributed representations. Section 3 introduces the experimental setting and presents the empirical contrast between quantization robustness and sparsity sensitivity. Section 4 develops the geometric interpretation of the learned representation, including the origin of the bimodal distribution, the Walsh influence analysis, and the scaling behavior under quantization. Section 5 provides additional experimental validation of the proposed interpretation. Finally, Section 6 discusses broader implications of the results, and Section 7 concludes the paper.

2. Related Work

Our study on compressing kernel associative memories relates to three research areas: low-precision deep learning, distributed representations, and the neurobiology of synaptic precision.

2.1 Low-Precision Deep Learning

Low-precision inference has been widely studied in deep learning. Binarized Neural Networks have shown that weights can be reduced to 1-bit without substantial loss of accuracy in complex tasks [5, 6]. More recently, 1.58-bit quantization in Large Language Models (e.g., BitNet [4]) has demonstrated the effectiveness of extreme compression. Our work extends these results from feedforward models to recurrent, kernel-based associative memories, showing that comparable robustness can be achieved.

2.2 Holographic and Distributed Representations

The concept of "holographic" representation, in which information is distributed rather than localized, has a long history. It is related to Holographic Reduced Representations [7] and the broader framework of Vector Symbolic Architectures [8, 9]. In these models, information is encoded across high-dimensional vectors, enabling superposition and retrieval.

In this paper, we define a representation as "holographic" if it satisfies two properties: (1) information is distributed across parameters, making the system sensitive to sparsity, and (2) the system is robust to local perturbations, such as low-precision quantization. Our results suggest that KLR learning yields a coding scheme consistent with these properties.

2.3 Biological Plausibility of Low-Precision Synapses

From a physiological perspective, the present results are consistent with principles of neural computation in the brain. Biological systems operate with noisy and imprecise components. Bartol et al. [10] provided nanoconnectomic evidence that hippocampal synapses operate with low precision (approximately 4.7 bits). This observation suggests that biological systems, similar to the KLR model considered here, rely on low-precision distributed representations rather than high-precision localized encoding.

3. Preliminaries and Empirical Phenomena

In this section, we briefly review the kernel Hopfield network model and the compression techniques used in this study. We then present the empirical observations that motivate the theoretical analysis, focusing

on the contrast between robustness to quantization and sensitivity to sparsity.

3.1 Kernel Hopfield Network and the Ridge of Optimization

The network consists of N neurons with state $\boldsymbol{s} \in \{-1, 1\}^N$, storing P patterns $\{\boldsymbol{\xi}^\mu\}_{\mu=1}^P$. The dual variables $(\alpha_{\mu i})_{1\le\mu\le P,\, 1\le i\le N}$ are learned via Kernel Logistic Regression (KLR) [11] using the RBF kernel $K(\boldsymbol{x}, \boldsymbol{y}) = \exp(-\gamma\|\boldsymbol{x} - \boldsymbol{y}\|^2)$. The retrieval dynamics are governed by the input potential:

$$h_i(\boldsymbol{s}) = \sum_{\mu=1}^{P} \alpha_{\mu i} K(\boldsymbol{s}, \boldsymbol{\xi}^\mu). \tag{1}$$

For the experiments, we focus on a regime identified in previous work, termed the "Ridge of Optimization" [3]. This region corresponds to a narrow band in the $(\gamma, P/N)$ phase space where attractor stability is maximized under high-load conditions. Unless otherwise noted, we use $P/N = 3.0$ and $\gamma = 0.02$, which were shown to yield both high capacity and stability.

3.2 Compression Schemes and Performance Metrics

3.2.1 Compression Schemes

To evaluate redundancy in the learned weights $\alpha_{\mu i}$, we apply two compression techniques post-training.

1. Uniform Quantization: We apply element-wise uniform quantization to the weight matrix $\boldsymbol{A} := (\alpha_{\mu i})$. Let x denote a weight element. The quantized value $Q_k(x)$ with k-bit precision is defined as:

$$Q_k(x) = \Delta \cdot \text{round}\left(\frac{x - x_{\min}}{\Delta}\right) + x_{\min}, \tag{2}$$

where $x_{\min}$ and $x_{\max}$ denote the minimum and maximum values of $\boldsymbol{A}$, and $\Delta = (x_{\max} - x_{\min})/(2^k - 1)$. We evaluate $k \in \{32, 16, \ldots, 2, 1\}$. For $k = 1$, we use the sign of the weights relative to the mean or median.

2. Magnitude Pruning (Sparsification): We induce sparsity by removing weights with small magnitude. For a target sparsity ratio $S \in [0, 1)$, we define a threshold τ such that a fraction S of the elements in $\boldsymbol{A}$ satisfy $|\alpha_{\mu i}| < \tau$. The pruned matrix $\boldsymbol{A}_p$ is defined as:

$$\boldsymbol{A}_p = \boldsymbol{A} \odot \mathbb{I}(|\boldsymbol{A}| \ge \tau), \tag{3}$$

where $|\cdot|$ and $\ge$ are applied element-wise, $\odot$ denotes the Hadamard product, and $\mathbb{I}(\cdot)$ is the indicator function.

3.2.2 Performance Metrics

- **Bit Accuracy:** The proportion of neurons whose updated states correctly match the corresponding stored pattern $\boldsymbol{\xi}^\mu$ after a single update step from $\boldsymbol{s} = \boldsymbol{\xi}^\mu$.
- **Bit-wise Recall Accuracy:** The proportion of neurons in the converged state that correctly match the target pattern when the dynamics are initialized from a noisy input.
- **Stability Margin:** The mean alignment $h_i(\boldsymbol{\xi}^\mu)\xi_i^\mu$, where larger positive values indicate greater robustness to perturbations.

3.3 Experimental Setup

All simulations were implemented in Python 3.13 using the `NumPy` 2.1.3 and `SciPy` 1.15.2 libraries. The experiments were conducted on a workstation equipped with an Intel Core i9-9900K CPU and 64 GB of RAM. No GPU acceleration was used.

Unless otherwise stated, all reported results are averaged over 10 independent trials with different random pattern realizations. For the recall experiments, noisy initial states were generated by randomly flipping a specified fraction of bits in the target pattern.

3.4 Empirical Observations: A Fundamental Dichotomy

To examine the learned representation, we apply both compression schemes to networks trained on the Ridge. While the main analysis uses $P/N = 3.0$, similar behavior is observed for other settings (e.g., $P/N = 2.0$; see Appendix B).

Robustness to Quantization: Figure 1 shows bit accuracy and stability margin as functions of the quantization bit depth k. The network maintains perfect recall accuracy even at 2-bit resolution, with negligible variance across trials. At $k = 1$, accuracy remains high.

The stability margin increases at low bit depths. This effect, termed *Quantization Saturation*, can be interpreted as saturation-induced amplification: discretization pushes small weights toward extreme values, increasing the magnitude of the input potential while preserving its sign.

Sensitivity to Sparsity: In contrast, Figure 2 shows that performance degrades rapidly as the sparsity ratio increases. Even moderate pruning (e.g., 10%) leads to a significant drop in accuracy, indicating that small-magnitude weights contribute to the representation.

Taken together, these results indicate qualitatively different responses to the two compression schemes. The network remains robust to aggressive quantization, while showing substantial sensitivity to sparsification. This contrast motivates the theoretical analysis in the following section.

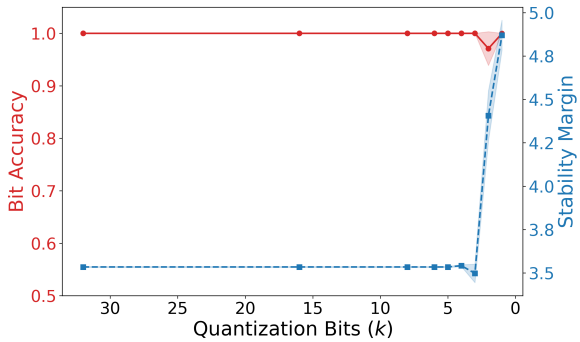

Fig. 1. Robustness to Uniform Quantization. Bit accuracy (red solid line) and stability margin (blue dashed line) as a function of quantization bit depth k. Shaded areas indicate standard deviation over 10 trials.

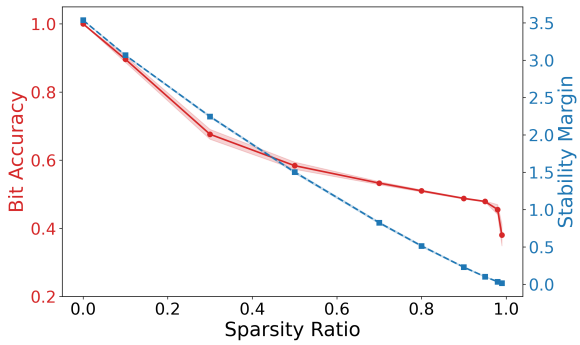

Fig. 2. Sensitivity to Magnitude Pruning. Performance metrics as a function of sparsity ratio (fraction of zeroed weights). Shaded areas indicate standard deviation over 10 trials.

3.5 Problem Formulation

These contrasting responses to the two compression schemes raise a central question. If the network is robust to quantization, why is it sensitive to pruning? Addressing this question requires an analysis of the geometric structure of the learned representation, which is developed in the next section.

4. Theoretical Analysis of Representation Geometry

In this section, we analyze the geometric structure of the learned representation from complementary viewpoints. Section 4.1 presents an interpretation of the emergence of a bimodal weight distribution based on symmetry breaking. Section 4.2 analyzes the functional structure in the input space using Walsh influence analysis, clarifying the distinction between functional sparsity and dense parameterization. Section 4.3 summarizes the resulting dual representation. Finally, Section 4.4 provides quantitative support for this interpretation by examining the scaling behavior of performance degradation under quantization.

4.1 Origin of Bimodal Distribution: A Force-Balance Model

The emergence of a bimodal weight distribution (Fig. 6), which contributes to robustness against quantization, can be interpreted through a force-balance model analogous to symmetry breaking in parameter space. The KLR learning objective consists of two competing components acting on the dual variables $\boldsymbol{A} = (\alpha_{\mu i})$:

1. **Attractive Effect (from L_2 Regularization):** The weight decay term ($\lambda \|\boldsymbol{A}\|_K^2$) creates a tendency that pulls the weights toward the origin ($\boldsymbol{A} = \mathbf{0}$), favoring a unimodal Gaussian-like distribution. This corresponds to a symmetric state in which the model has no preference for any particular feature direction.
2. **Repulsive Effect (from Margin Maximization):** The logistic loss term seeks to maximize the classification margin by driving the weights toward large positive or negative values. This effect tends to break the symmetry around the origin, separating the parameters into positive and negative clusters to ensure pattern separability under high load.

During learning on the Ridge of Optimization, we hypothesize that these two competing effects reach a delicate balance. The repulsive contribution from the data term becomes sufficiently strong to overcome the attraction toward zero, potentially rendering the symmetric state at $\boldsymbol{A} = \mathbf{0}$ unstable. Consequently, the system is expected to settle into one of two stable non-zero states, forming an effective double-well-like structure in the weight distribution.

This interpretation provides a possible explanation for the emergence of a bimodal distribution without explicit binarization constraints, in which the parameters effectively take near-discrete values. The empirical validation of this bimodal distribution is presented in Sec. 5.2.

4.2 Holographic vs. Sparse Influence: A Walsh Analysis

Our results indicate a characteristic property of the memory representation on the Ridge, which was previously associated with the state of *Spectral Concentration* [3].

The sensitivity to sparsity pruning (Fig. 2) motivates a closer examination of the information structure of the learned representation. To investigate this quantitatively, we employ Walsh analysis, a set of Fourier-analytic tools for analyzing Boolean functions [12].

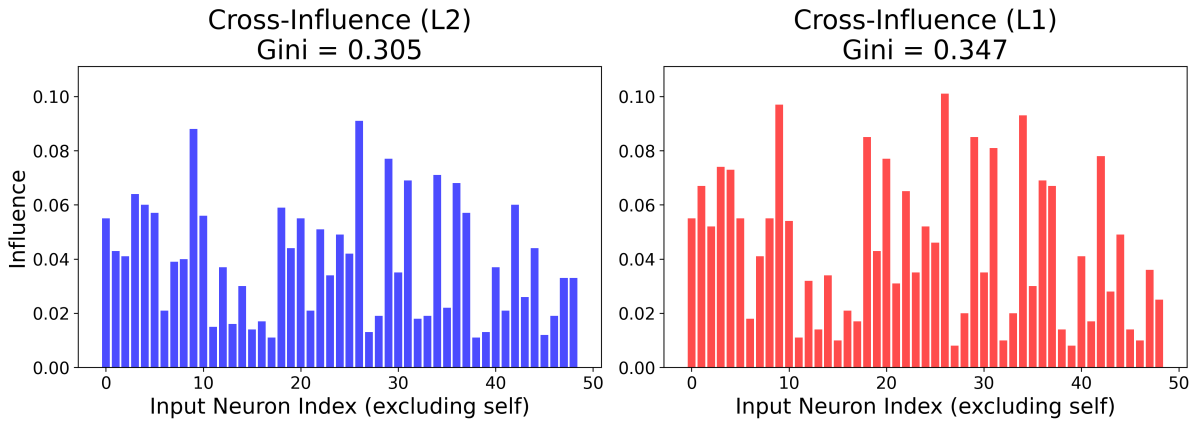

Fig. 3. Input Influence Distribution for L_2 vs. L_1 Regularization. The plots show the influence of each input neuron on the output of a single target neuron, estimated via Walsh analysis. (Left) The standard KLR model (L_2) retains a dense tail of cross-influences. (Right) The L_1-regularized (Lasso) model shows a much sparser influence profile.

We treat the update function $h_j(\boldsymbol{s})$ for a single output neuron j as a mapping $\{-1, 1\}^N \to \mathbb{R}$ and compute the influence of each input neuron s_i. The influence $I_i(h_j)$ measures the probability that flipping input s_i changes the sign of the output h_j, thereby quantifying its functional importance.

We compared the influence distribution of the standard KLR model (L_2 regularization) with that of a model trained using L_1 regularization (Lasso), which explicitly promotes sparsity. To isolate the effect of inter-neuron couplings, we analyzed the "cross-influence" by excluding the dominant self-influence term ($i = j$). The results are shown in Fig. 3.

Contrary to a naive holographic interpretation, which would predict a uniform influence distribution, both models exhibit a sparse influence structure, indicating that the KLR network performs a form of feature selection. However, an important quantitative difference appears in the tail behavior of the influence distribution. The L_2-regularized model (left panel of Fig. 3) retains a richer and denser tail of small cross-influences, yielding a Gini coefficient of $G \approx 0.305$. In contrast, the L_1-regularized model (right panel of Fig. 3) exhibits a more unequal distribution with a higher Gini coefficient of $G \approx 0.347$.

These results suggest that, although the effective input-output mapping exhibits sparse characteristics, the underlying parameterization of the L_2 model remains more distributed. Together with its robustness to quantization, this behavior is consistent with the notion of a holographic representation discussed in Sec. 2, and helps explain the observed sensitivity to pruning.

4.3 Geometric Interpretation: Duality of Representation

This subsection integrates the preceding analyses into a unified geometric interpretation of the learned representation. Combining the analyses of the weight distribution and input influence, our results suggest a dual structure in the KLR memory representation:

- **Parameter Space (Digital & Dense):** The weights $\boldsymbol{A}$ self-organize into a bimodal, digital-like structure. This representation appears to be dense rather than sparse, which may underlie its sensitivity to pruning. At the same time, its intrinsic discreteness makes it highly robust to quantization.
- **Input Space (Sparse Influence):** The function computed by the network exhibits sparse input dependencies. This suggests that the network selectively relies on a subset of informative features, consistent with effective feature learning.

This dual structure provides an interpretation of the contrasting effects of compression. While the effective input-output mapping exhibits sparse characteristics, the underlying parameterization remains distributed. In the sense discussed in Sec. 2, this behavior is consistent with a holographic representation at the parameter level.

The network appears to learn a sparse functional structure in the input space while implementing it through a dense and distributed parameterization in the feature space. This separation between functional sparsity and dense parameterization explains why quantization preserves performance whereas pruning

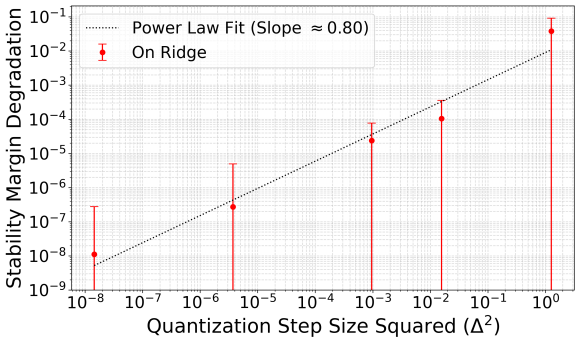

Fig. 4. Scaling Law of Quantization Error on the Ridge. The plot shows the degradation in Stability Margin as a function of the squared quantization step size (Δ^2) on a log-log scale. Error bars indicate standard deviation over 10 trials.

causes substantial degradation: quantization largely preserves the coarse distributed structure of the parameters, while pruning removes components that contribute to the distributed representation.

More broadly, this separation between sparse functional structure and dense parameterization may provide a useful perspective for understanding robust computation in neural systems.

4.4 Scaling Law of Quantization Error

This subsection does not introduce a new theoretical mechanism. Instead, it provides quantitative support for the geometric interpretation developed in the preceding subsections by examining how performance degradation scales with quantization strength.

Theoretically, under a local quadratic approximation of the loss landscape, the degradation is expected to scale quadratically with the quantization step size Δ (see Appendix A for a heuristic derivation). To test this hypothesis, we measured the degradation of the Stability Margin for a range of quantization bit depths $k \in \{16, 12, 10, 8, 7, 6, 5, 4, 3, 2\}$, both on and off the Ridge. While we focus on the Stability Margin as a sensitive probe, similar trends were observed for other performance metrics (not shown).

The results for the "On Ridge" regime are shown in Fig. 4. Data points are visible only where the degradation is positive; for higher bit depths, the degradation was negligible (zero or negative) and therefore omitted on the logarithmic scale. The visible points are consistent with a power-law relationship. A linear fit to the logarithmic data yields a slope of approximately 0.80, giving the empirical scaling relation:

$$\text{Degradation} \propto (\Delta^2)^{\beta}, \quad \text{with } \beta \approx 0.80. \tag{4}$$

Although this exponent deviates slightly from the ideal quadratic prediction ($\beta = 1$), the observed power-law scaling indicates that the degradation progresses in a predictable and gradual manner. In contrast, for the "Off Ridge (Local)" regime, the degradation was negligible across all bit depths, consistent with the flatter energy landscape in this region (see Appendix C for the detailed plot). This scaling analysis supports the interpretation that the geometric structure of the Ridge governs its robustness to parameter perturbations.

We conjecture that the deviation from the ideal exponent arises from finite-size effects and higher-order nonlinearities in the attractor geometry that are not captured by the quadratic approximation. Furthermore, the highly skewed spectrum of the Fisher information matrix reported for deep networks [13] suggests that the parameter space is strongly anisotropic. In such a geometry, quantization noise may be preferentially absorbed along flat directions associated with small eigenvalues, resulting in weaker degradation than predicted by the quadratic approximation. A more precise theoretical characterization of this exponent is left for future work.

5. Experimental Validation

The theoretical analysis in the previous section proposed a dual structure of the KLR representation: a bimodal structure in parameter space and sparse influence in the input space. In this section, we provide further experimental evidence supporting these theoretical interpretations.

5.1 Preservation of Basin Depth under Quantization

Our theory suggests that the bimodal, discrete-like nature of the weights should make the attractor landscape robust to quantization. To examine this, we evaluated the noise robustness of the quantized network.

Figure 5 compares the bit-wise recall accuracy of the full-precision (Float32) and 2-bit quantized models as a function of input noise level. The performance of the 2-bit model closely tracks that of the full-precision baseline, maintaining high accuracy even under significant corruption (e.g., > 85% accuracy at 20% noise). These results indicate that quantization largely preserves the attractor basin structure, consistent with the discrete parameter organization discussed in Sec. 4.1.

5.2 Empirical Evidence of Bimodal Weight Distribution

A central component of our theoretical interpretation is the spontaneous emergence of a bimodal weight distribution, modeled in Sec. 4.1 as the result of com-

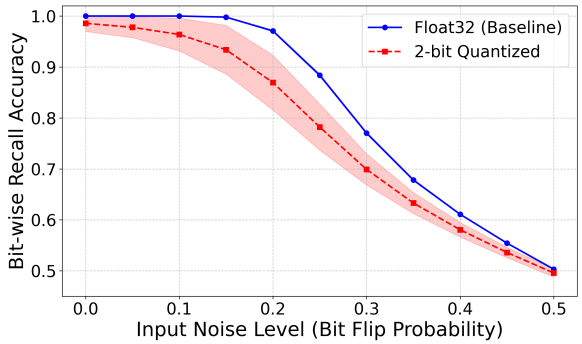

Fig. 5. Noise Robustness Comparison (Bit-wise Accuracy). Recall performance as a function of input noise level (bit flip probability). Shaded areas indicate standard deviation over 10 trials.

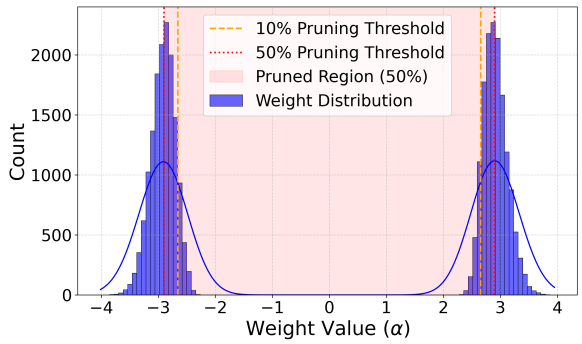

Fig. 6. Weight Distribution on the Ridge. The learned weights exhibit a distinct bimodal distribution, concentrating around two non-zero values (±3.0) with very few weights near zero.

peting effects in the learning objective. To examine this hypothesis, we analyzed the empirical distribution of the learned weights $\boldsymbol{A}$ on the Ridge ($\gamma = 0.02$, $P/N = 3.0$).

Figure 6 shows the histogram of the weight elements. Consistent with the proposed force-balance interpretation, the distribution is not unimodal. Instead, it separates into two clusters centered around non-zero values (approximately ±3.0), with relatively few weights near the origin. This observation is consistent with the interpretation of an effective double-well-like structure governing the weight distribution.

Furthermore, the observed distribution provides an intuitive explanation for the sensitivity to magnitude pruning. Since only a small fraction of weights are located near zero, pruning preferentially removes weights from the tails of the two clusters, where they still contribute to the distributed representation.

5.3 The Ridge as a Robust Operating Region

Our theoretical interpretation suggests that the geometric structure of the Ridge plays a central role in quantization robustness. To examine this hypothesis, we investigated how quantization sensitivity changes

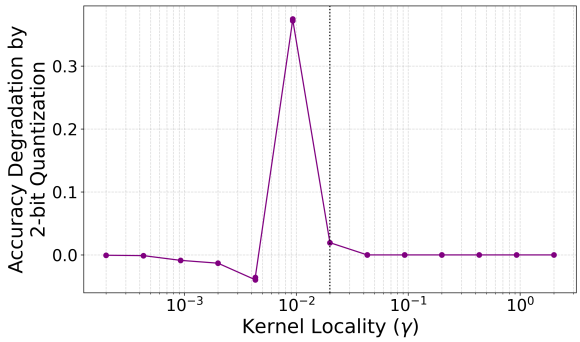

Fig. 7. Quantization Sensitivity vs. Kernel Locality. The plot shows the accuracy degradation caused by 2-bit quantization as a function of the kernel locality parameter γ. The Ridge center ($\gamma^* = 0.02$, vertical dotted line) is located in a robust region.

as the kernel parameter moves away from the Ridge center ($\gamma^* = 0.02$). Specifically, we measured the accuracy degradation induced by 2-bit quantization for various γ values while fixing the load at $P/N = 3.0$.

The results are shown in Fig. 7. The plot reveals an asymmetric valley-like structure. In the local regime ($\gamma > \gamma^*$), the accuracy degradation remains nearly zero, consistent with the smaller weight magnitudes in this regime and their reduced sensitivity to discretization. In contrast, the most pronounced feature appears in the global regime ($\gamma < \gamma^*$). As γ decreases from the Ridge center, the degradation rapidly increases and reaches a sharp peak around $\gamma \approx 0.01$, corresponding to catastrophic retrieval failure.

This peak likely corresponds to the capacity boundary of the network. Near this critical region, the system becomes highly sensitive to parameter perturbations, and quantization can induce a complete collapse of retrieval performance. The region further to the left ($\gamma < 0.01$) corresponds to an overloaded phase in which even the full-precision model fails to learn stable memories properly.

Overall, these results suggest that the Ridge of Optimization is not merely a point of minimal quantization error, but rather a robust operating region located near the transition to memory overload.

6. Discussion

Our analysis, combining empirical observations with theoretical modeling and experimental validation, suggests that KLR networks employ a structured form of information representation. The present results were obtained near the Ridge of Optimization, which we regard as a structurally important regime for high-capacity kernel models. However, the compression behavior outside this regime remains an open question.

6.1 The Duality of Representation

The central theoretical finding of this paper is the dual nature of the memory representation. The Walsh analysis (Sec. 4.2) showed that the network learns a sparse input mapping, effectively performing feature selection. In contrast, the parameter representation in the feature space remains dense and holographic, as indicated by its sensitivity to pruning (Sec. 3.4). This duality suggests a trade-off between efficiency and robustness: the network identifies a relatively small set of informative features while encoding them in a distributed and fault-tolerant manner. This principle may extend beyond associative memory to more general forms of neural computation.

6.2 Spectral Bias and Memory Stability

Recent studies by Karakida et al. [13, 14] have identified a structural property commonly observed in deep neural networks: the Fisher information matrix often exhibits a highly skewed spectrum dominated by a small number of large eigenvalues. Although such spectral structure is sometimes described as "pathological," our results suggest an alternative interpretation in the context of associative memory.

We hypothesize that KLR learning near the Ridge accentuates this intrinsic spectral bias. By exploiting the dominant spectral modes, the system may efficiently form deep and stable attractor basins, while suppression of the bulk spectrum reduces inter-pattern interference. From this perspective, a spectral bias that may be detrimental in other learning contexts instead becomes advantageous for associative memory storage. This property may also reflect a physiological principle underlying robust and high-capacity memory. This interpretation further motivates the biological perspective discussed in Sec. 6.4.

6.3 The Ridge as a Critical Operating Regime

Our scaling analysis (Sec. 4.4) and distance-to-ridge analysis (Sec. 5.3) provide a more nuanced characterization of the Ridge of Optimization. The Ridge is not merely a point of maximal stability, but rather a critical operating regime that balances multiple trade-offs. The observed power-law scaling suggests that the landscape is geometrically smooth, allowing gradual performance degradation under quantization. At the same time, the proximity of the Ridge to the capacity boundary suggests that the system self-organizes near a transition between stable retrieval and memory failure, a behavior reminiscent of Self-Organized Criticality [15].

From this perspective, the Ridge may represent a favorable operating region that combines high performance with robustness against catastrophic degradation. Practically, this state may be identified by monitoring geometric metrics such as Pinnacle Sharpness [3], or more simply, by observing the emergence of a bimodal weight distribution during training.

6.4 Revisiting Biological Plausibility

The holographic and low-precision characteristics of the KLR representation are consistent with several principles of neural coding in biological systems. Neural systems are thought to operate robustly despite noisy and low-precision synaptic components [16]; for example, hippocampal synapses have been estimated to possess a precision of only a few bits [10]. Our results suggest that the combination of a dense and distributed representation (holographic) with a low-precision digital format (e.g., 2-bit quantization) provides a robust mechanism for memory representation.

Although the KLR learning algorithm itself is not biologically plausible, the resulting geometric structure, namely a bimodal and fault-tolerant weight distribution, may reflect a convergent solution shared by both artificial and biological learning systems.

6.5 Practical Implications for Hardware

The findings of this study suggest several implications for hardware-efficient implementation. In particular, the combination of quantization robustness and a dense holographic representation enables substantial reductions in memory and computational cost. Robustness to 2-bit quantization yields a 16-fold reduction in memory footprint relative to standard 32-bit floating-point storage. For example, a network with $N = 1000$ and $P = 3000$ would normally require approximately 12 MB of memory, whereas 2-bit quantization reduces this requirement to approximately 0.75 MB. This reduction may allow the entire model to fit within the on-chip SRAM of low-power edge devices.

Furthermore, the retrieval computation can be accelerated through low-precision arithmetic. By quantizing weights to 1-bit or 2-bit, floating-point multiply-accumulate operations can be replaced by bitwise XNOR and population count operations. Such binary operations have been reported to achieve substantial computational efficiency [5]. While sparsity is often used to reduce computational cost, our results suggest that, for high-capacity associative memory, low-precision dense computation may provide a more favorable trade-off between computational efficiency and memory performance.

In addition to reducing memory and computational cost, quantization may also improve energy efficiency. A 32-bit floating-point multiplication consumes approximately 3.7 pJ of energy on a 45 nm process, whereas a binary XNOR operation consumes less than 0.1 pJ [17]. For large-scale associative memory with millions of parameters, this difference may translate into substantial reductions in power consumption, which is particularly important for battery-operated edge devices.

6.6 Limitations and Future Work

The present study focuses primarily on the recall of random binary patterns. How structural correlations in real-world data (e.g., images or language representations) may affect the "duality" principle proposed here remains an important subject for future investigation. Furthermore, the present analysis is limited to post-training quantization. Extending the proposed geometric framework to quantization-aware training is another important direction for future work.

7. Conclusion

In this work, we presented a geometric interpretation of the compression robustness observed in high-capacity KLR Hopfield networks. Our analysis showed that the contrasting responses to quantization and sparsity arise from a dual representation: a dense, bimodal structure in parameter space and a sparse functional mapping in the input space.

From a theoretical perspective, we interpreted the emergence of this structure through a spontaneous symmetry breaking mechanism. Empirically, quantitative scaling analysis revealed a predictable power-law relationship governing the degradation induced by quantization. Our findings further suggest that the "Ridge of Optimization" is not merely a high-performance region, but a critical operating regime located near the transition to memory overload. In this regime, the network combines geometric stability with high memory capacity. The principle of "sparse function, dense representation" may therefore provide a useful perspective for understanding robust and efficient computation in both artificial and biological neural systems.

Finally, the present results suggest that kernel-based associative memories may be implemented efficiently on low-power hardware through low-precision quantization. Significant reductions in memory usage and computational cost are achievable while largely preserving retrieval performance. These findings indicate that KLR Hopfield networks are a promising candidate for neuromorphic and edge-oriented memory systems.

Funding

Not applicable.

Conflicts of interest

The author declares no competing interests.

Author contribution

The sole author contributed to the present work.

Artificial intelligence tools

The author used ChatGPT (GPT-5.3) and Gemini 2.5 Pro for proofreading the English manuscript.

Appendix

A. Heuristic Derivation of Quadratic Scaling

Here, we provide a heuristic argument for why the performance degradation is expected to scale quadratically with the quantization step size, i.e., Degradation $\propto \Delta^2$.

Let $L(\boldsymbol{A})$ denote the loss function. Under the assumption that the loss landscape is smooth and locally approximated by a second-order Taylor expansion around an optimum $\boldsymbol{A}^*$,

$$L(\boldsymbol{A}^* + \boldsymbol{\delta}) \approx L(\boldsymbol{A}^*) + \nabla L(\boldsymbol{A}^*)^\top \boldsymbol{\delta} + \frac{1}{2}\boldsymbol{\delta}^\top \boldsymbol{H}\boldsymbol{\delta}, \quad \text{(A-1)}$$

where $\boldsymbol{\delta} = Q_k(\boldsymbol{A}) - \boldsymbol{A}^*$ denotes the quantization error vector and $\boldsymbol{H}$ is the Hessian matrix (or the Fisher information matrix). Since $\boldsymbol{A}^*$ corresponds to a local minimum, the gradient term $\nabla L(\boldsymbol{A}^*)$ is approximately zero. The increase in loss is therefore approximated as

$$\Delta L = L(Q_k(\boldsymbol{A})) - L(\boldsymbol{A}^*) \approx \frac{1}{2}\boldsymbol{\delta}^\top \boldsymbol{H}\boldsymbol{\delta}. \quad \text{(A-2)}$$

Uniform quantization introduces a rounding error for each parameter, which is uniformly distributed over the interval $[-\Delta/2, \Delta/2]$. The mean squared error for a single parameter is therefore

$$\mathbb{E}[\delta_i^2] = \frac{1}{\Delta}\int_{-\Delta/2}^{\Delta/2} x^2\, dx = \frac{\Delta^2}{12}. \quad \text{(A-3)}$$

Assuming that the quantization errors are uncorrelated across the $D = P \times N$ dimensions, the expected increase in loss becomes

$$\begin{aligned} \mathbb{E}[\Delta L] &\approx \frac{1}{2}\mathbb{E}\left[\sum_i \sum_j H_{ij}\delta_i\delta_j\right] \\ &= \frac{1}{2}\sum_i H_{ii}\mathbb{E}[\delta_i^2] \\ &= \frac{1}{2}\mathrm{Tr}(\boldsymbol{H})\frac{\Delta^2}{12}. \end{aligned} \quad \text{(A-4)}$$

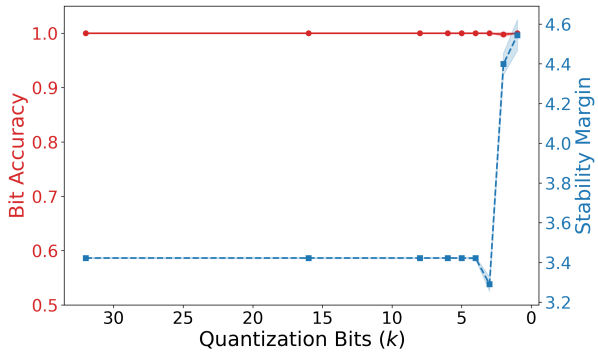

(a) Quantization Robustness

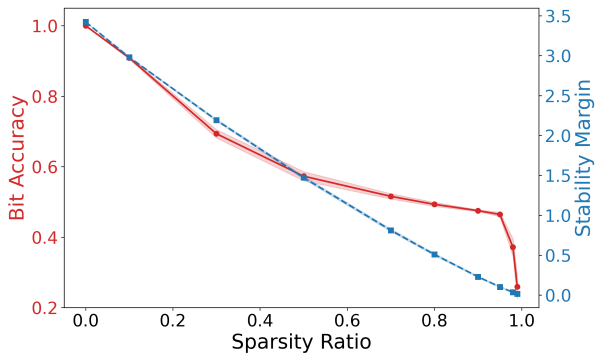

(b) Sparsity Sensitivity

Fig. B-1. Performance of the compressed network at a lower storage load of $P/N = 2.0$. Shaded areas indicate standard deviation over 10 trials.

If the performance degradation (e.g., the loss of stability margin) is monotonically related to the increase in loss, then the degradation is expected to scale proportionally with Δ^2:

$$\text{Degradation} \propto \mathbb{E}[\Delta L] \propto \Delta^2. \tag{A-5}$$

Despite its simplifying assumptions, this model provides a heuristic interpretation of the power-law scaling observed in our experiments and explains the origin of the quadratic dependence.

B. Generality Across Storage Loads

To confirm that the observed behavior is not specific to the high-load condition of $P/N = 3.0$, we repeated the compression experiments at a lower, yet still challenging, storage load of $P/N = 2.0$. The results, shown in Fig. B-1, exhibit the same qualitative trends.

The network maintains perfect bit accuracy down to 2-bit quantization, whereas performance degrades rapidly under sparsity pruning. The weight distribution (not shown) also remains bimodal. These results suggest that the "sparse function, dense representation" structure is a robust property of the Ridge of Optimization across multiple high-load conditions, rather than an artifact of a particular hyperparameter setting.

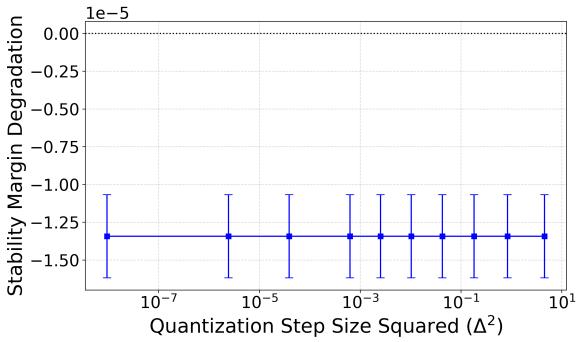

Fig. C-1. Stability margin degradation in the Local regime ($\gamma = 0.1$). The data points show the mean degradation over 10 trials, and the error bars indicate the standard deviation. The degradation remains negligible across all tested quantization levels.

C. Quantization Behavior in the Local Regime

To complement the scaling analysis presented in Sec. 4.4, this appendix provides the detailed results for the "Off Ridge (Local)" regime. As shown in Fig. C-1, the degradation of the stability margin remains close to zero (or slightly negative) across all tested bit depths. This indicates that the network in the local regime is largely insensitive to parameter quantization, in contrast to the predictable power-law degradation observed near the Ridge.

References

[1] A. Tamamori, "Kernel logistic regression learning for high-capacity hopfield networks," *IEICE Trans. Inf. & Syst.*, vol. E109-D, no. 2, pp. 293–297, February 2026. DOI:10.1587/transinf.2025EDL8027

[2] A. Tamamori, "Quantitative attractor analysis of high-capacity kernel hopfield networks," *NOLTA*, vol. E17-N, no. 3, July 2026. (in press)

[3] A. Tamamori, "Self-organization and spectral mechanism of attractor landscapes in high-capacity kernel hopfield networks," *NOLTA*, vol. E17-N, no. 3, July 2026. (in press)

[4] S. Ma, H. Wang, L. Ma, L. Wang, W. Wang, S. Huang, L. Dong, R. Wang, J. Xue, and F. Wei, "The era of 1-bit llms: all large language models are in 1.58 bits," arXiv preprint:arXiv:2402.17764, February 2024. DOI:10.48550/arXiv.2402.17764

[5] M. Rastegari, V. Ordonez, J. Redmon and A. Farhadi, "Xnor-net: imagenet classification using binary convolutional neural networks," Proc. ECCV'16, September 2016. DOI:10.1007/978-3-319-46493-0_32

[6] I. Hubara, M. Courbariaux, D. Soudry, R. El-Yaniv, and Y. Bengio, "Binarized neural networks," Proc. NIPS'16, pp. 4114–4122, December 2016.

[7] T.A. Plate, "Holographic reduced representations," *IEEE Transactions on Neural Networks*, vol. 6, no. 3, pp. 623–641, May 1995. DOI:10.1109/72.377968

[8] P. Kanerva, "Hyperdimensional computing: an introduction to computing in distributed representation with high-dimensional random vectors," *Cognitive Computation*, vol. 1, pp. 139–159, June 2009. DOI:10.1007/s12559-009-9009-8

[9] R.W. Gayler, "Vector symbolic architectures answer jackendoff's challenges for cognitive neuroscience," Proc. ICCS'03, pp. 133–138, July 2003.

[10] T.M. Bartol Jr., C. Bromer, J. Kinney, M.A. Chirillo, J.N. Bourne, K.M. Harris, and T.J. Sejnowski, "Nanoconnectomic upper bound on the variability of synaptic plasticity," *eLife*, vol. 4, pp. e10778, November 2015. DOI:10.7554/eLife.10778

[11] B. Schölkopf and A.J. Smola, *Learning with Kernels: Support Vector Machines, Regularization, Optimization, and Beyond*, MIT Press, 2001. DOI:10.7551/mitpress/4175.001.0001

[12] R. O'Donnell, *Analysis of Boolean Functions*, Cambridge University Press, July 2014. DOI:10.1017/CBO9781139814782

[13] R. Karakida, S. Akaho, and S. Amari, "Universal statistics of fisher information in deep neural networks: mean field approach," *Journal of Statistical Mechanics: Theory and Experiment*, vol. 2020, no. 12, pp. 124005, December 2020. DOI:10.1088/1742-5468/abc62e

[14] R. Karakida, S. Akaho, and S. Amari, "Pathological spectral of the fisher information metric and its variants in deep neural networks," *Neural Computation*, vol. 33, no. 8, pp. 2274–2307, July 2021. DOI:10.1162/neco_a_01411

[15] J.M. Beggs, D. Plenz, "Neuronal Avalanches in Neocortical Circuits," *Journal of Neuroscience*, vol. 23, no. 35, pp. 11167–11177, December 2003. DOI:10.1523/JNEUROSCI.23-35-11167.2003

[16] F. Rieke, D. Warland, R. Steveninck, and W. Bialek, *Spikes: Exploring the Neural Code*, MIT Press, December 1996.

[17] M. Horowitz, "1.1 Computing's energy problem (and what we can do about it)," Proc. ISSCC'14, vol. 57, pp. 10–14, March 2014. DOI:10.1109/ISSCC.2014.6757323